

Bulk Electronic State of Superconducting Topological Insulator

Tatsuki Hashimoto, Keiji Yada, Ai Yamakage, Masatoshi Sato and Yukio Tanaka

Department of Applied Physics, Nagoya University, Nagoya 464-8603, Japan

We study the electronic properties of a superconducting topological insulator whose parent material is a topological insulator. We calculate the temperature dependence of the specific heat and spin susceptibility for four promising superconducting pairings proposed by L. Fu and E. Berg [Phys. Rev. Lett. **105** (2010) 097001]. Since the line shapes of the temperature dependence of specific heat are almost identical among three of the four pairings, it is difficult to identify them simply from the specific heat. On the other hand, we obtain wide variations of the temperature dependence of spin susceptibility for each pairing, reflecting the spin structure of the Cooper pair. We propose that the pairing symmetry of a superconducting topological insulator can be determined from measurement of the Knight shift by changing the direction of the applied magnetic field.

KEYWORDS: superconducting topological insulator, topological superconductor, topological insulator, unconventional superconductivity, odd-parity, spin-orbit interaction, multi-band system, spin susceptibility, specific heat

1. Introduction

Topological insulators (TIs) are a newly discovered state of matter supporting massless Dirac fermions on the surface and characterized by nonzero topological numbers defined in the bulk.^{1,2)} Because of the presence of the surface Dirac fermions, TIs have the potential to exhibit rich transport and electromagnetic response properties, which may be applicable for future devices. The superconducting analog of TIs are topological superconductors,²⁻⁶⁾ which have Majorana fermions⁷⁾ on the surface as Andreev bound states (ABSs). In these materials, topological invariants can be defined in the bulk Hamiltonian. There are several types of topological superconductors, e.g., the chiral p -wave superconducting state in Sr_2RuO_4 ⁸⁻¹²⁾ and the helical superconducting state realized in non-centrosymmetric superconductors.^{13,14)} The realization of a topological superconductor is of particular interest from the viewpoint of quantum devices and quantum computations.¹³⁻³²⁾

Recently, the carrier-doped TI $\text{Cu}_x\text{Bi}_2\text{Se}_3$ has been revealed to be a superconductor.³³⁾ Hereafter, we refer to a superconductor based on a TI as a superconducting topological insulator (STI). In tunneling spectroscopy,³⁴⁾ $\text{Cu}_x\text{Bi}_2\text{Se}_3$ shows a zero-bias conductance peak (ZBCP). This means that $\text{Cu}_x\text{Bi}_2\text{Se}_3$ can be regarded as a topological superconductor since the ZBCP signifies the existence of gapless ABSs³⁵⁻³⁷⁾ on the surface, which is a direct consequence of topological superconductivity. Interestingly, it has been clarified that an STI supports anomalous ABSs different from those of other topological superconductors,^{30,38,39)} and the resulting transport property also becomes anomalous.^{30,39)} In this sense, STIs are a new type of topological superconductor, and have attracted much interest. Moreover, there are several experimental results supporting the generation of an STI by the

proximity effect,^{40,41)} while a recent study based on scanning tunneling spectroscopy has reported conventional superconductivity in an STI.⁴²⁾

There have been many relevant studies on $\text{Cu}_x\text{Bi}_2\text{Se}_3$.^{33,34,43-49)} However, up to now, the symmetry of the superconductivity of $\text{Cu}_x\text{Bi}_2\text{Se}_3$ still remains unknown, while its topological properties crucially depend on the pairing symmetry. Although the specific heat has been measured, it is difficult to establish the superconducting symmetry only from the data of specific heat. More careful analysis with the help of microscopic calculations is needed. In order to clarify the superconducting symmetry, it is useful to analyze the spin susceptibility in addition to the specific heat since the spin susceptibility is directly related to the spin structure of the superconducting pairing. Indeed, to determine the pairing symmetry of unconventional superconductors such as cuprates, Sr_2RuO_4 and UPt_3 , the measurement of specific heat and spin susceptibility has played an important role.^{8,9,50-56)}

In this paper, we clarify the temperature dependence of specific heat and spin susceptibility for the possible superconducting pairings. In contrast to unconventional superconductors, because of the strong spin-orbit interaction, a mixture of orbital degrees of freedom is essential to realize unconventional superconductivity in an STI. Therefore, a careful analysis is needed to study the specific heat and spin susceptibility. Actually, we find that the quasi-particle spectra of an STI are very different from those of the previously studied unconventional superconductors, and thus the spin susceptibility depends on the d -vector nontrivially. In particular, even for a spin-singlet superconducting gap (Δ_3 in the text), an STI may show T -independent spin susceptibility. On the basis of the non trivial behaviors of the specific heat and spin suscep-

tibility, it is possible to determine the pairing symmetry in an STI.

The paper is organized as follows. In §2, we give the model Hamiltonian of an STI and the energy spectra for the possible superconducting pairings. The numerical results and discussion on the temperature dependences of the specific heat and spin susceptibility are given in §3 and §4, respectively. We compare our results of specific heat with the experimental data.⁴⁵⁾ In §5, we summarize our results and propose how to experimentally determine the superconducting symmetry of an STI.

2. Model

For our model of an STI, we start with the Bogoliubov-de Gennes (BdG) Hamiltonian proposed in ref. 57,

$$H(\mathbf{k}) = H_0(\mathbf{k})\tau_z + \Delta_\ell\tau_x, \quad (1)$$

where $\ell(= 1, 2, 3, 4)$ represents the type of pair potential. The normal part of the Hamiltonian $H_0(\mathbf{k})$ is the low-energy effective model of a topological insulator based on $\mathbf{k} \cdot \mathbf{p}$ theory given by

$$H_0(\mathbf{k}) = c(\mathbf{k}) + m(\mathbf{k})\sigma_x + v_z k_z \sigma_y + v(k_x s_y - k_y s_x)\sigma_z, \quad (2)$$

$$m(\mathbf{k}) = m_0 + m_1 k_z^2 + m_2(k_x^2 + k_y^2), \quad (3)$$

$$c(\mathbf{k}) = -\mu + c_1 k_z^2 + c_2(k_x^2 + k_y^2). \quad (4)$$

s_i , σ_i and τ_i ($i = x, y, z$) are the Pauli matrices in the spin, orbital and Nambu spaces respectively.] The basis of the orbitals consists of effective p_z orbitals constituted from the p_z orbitals of Se and Bi on the upper and lower sides of the quintuple layer, as shown in Fig. 1. Hereafter, we call this basis the ‘‘orbital basis’’. On the other hand, we refer to the basis diagonalizing $H_0(\mathbf{k})$ as the ‘‘band basis’’, which is introduced in §4.2. In this model, the normal part $H_0(\mathbf{k})$ is equivalent to the model proposed in refs. 58 and 59 under the unitary transformation. In the following, we use the tight-binding model, which is equivalent to the above model at low energy. We consider a hexagonal lattice where two-dimensional triangular lattices are stacked along the c -axis.^{34,38)} Then, the tight-binding Hamiltonian is obtained by the following substitution in the $\mathbf{k} \cdot \mathbf{p}$ Hamiltonian given by eqs. (2)-(4).

$$k_x \rightarrow \frac{2}{\sqrt{3}a} \sin \frac{\sqrt{3}k_x a}{2} \cos \frac{k_y a}{2} \equiv f_x(\mathbf{k}), \quad (5)$$

$$k_y \rightarrow \frac{2}{3a} \left(\cos \frac{\sqrt{3}k_x a}{2} \sin \frac{k_y a}{2} + \sin k_y a \right) \equiv f_y(\mathbf{k}), \quad (6)$$

$$k_z \rightarrow \frac{1}{c} \sin k_z c \equiv f_z(\mathbf{k}), \quad (7)$$

$$k_z^2 \rightarrow \frac{2}{c^2} (1 - \cos k_z c) \equiv f_\perp(\mathbf{k}), \quad (8)$$

$$k_x^2 + k_y^2 \rightarrow \frac{4}{3a^2} \left(3 - 2 \cos \frac{\sqrt{3}k_x a}{2} \cos \frac{k_y a}{2} - \cos k_y a \right)$$

$$\equiv f_\parallel(\mathbf{k}), \quad (9)$$

where a and c are the lattice constants. In this hexagonal lattice, the primitive lattice vectors are $(\sqrt{3}a/2, a/2, 0)$, $(0, a, 0)$, and $(0, 0, c)$, although the actual crystal structure is not hexagonal but rhombohedral.^{58,59)} This simplification does not affect the low-energy excitations. Then, the normal part of the Hamiltonian is summarized as follows:

$$H_0(\mathbf{k}) = c(\mathbf{k}) + m(\mathbf{k})\sigma_x + (a_x(\mathbf{k})s_y - a_y(\mathbf{k})s_x)\sigma_z + b(\mathbf{k})\sigma_y, \quad (10)$$

$$c(\mathbf{k}) = -\mu + c_1 f_\perp(\mathbf{k}) + c_2 f_\parallel(\mathbf{k}), \quad (11)$$

$$m(\mathbf{k}) = m_0 + m_1 f_\perp(\mathbf{k}) + m_2 f_\parallel(\mathbf{k}), \quad (12)$$

$$a_{x,y}(\mathbf{k}) = v f_{x,y}(\mathbf{k}), \quad (13)$$

$$b(\mathbf{k}) = v_z f_z(\mathbf{k}). \quad (14)$$

Here, we choose the chemical potential $\mu = 0.5$ eV, since the chemical potential measured from the surface Dirac point is 0.4-0.5 eV according to ref. 43. We use the values of the parameters c_2 , m_0 , m_2 and v as given in ref. 59. On the other hand, for c_1 , m_1 and v_z , we choose the different values given in ref. 59, which involve hopping along the c -axis. Since the parameterization performed in ref. 59 is based on the dispersion around the Γ -point, the difference in the dispersion near the zone boundary between the first-principles calculation in ref. 59 and our tight-binding model is considerably large. However, the Fermi surface becomes cylindrical if we use the same parameters given in ref. 59 although the correct shape of the Fermi surface is an spheroidal one. Thus, we choose the values of c_1 , m_1 and v_z as $c_1/c^2 = 0.024$, $m_1/c^2 = 0.216$ and $v_z/c = 0.32$ (eV) to fit the energy dispersion for the Γ -Z direction obtained in ref. 59. These parameters give the spheroidal Fermi surface consistent with the first-principles calculation. This parameterization is crucial since the specific heat and spin susceptibility in actual $\text{Cu}_x\text{Bi}_2\text{Se}_3$ cannot be reproduced if we use a cylindrical Fermi surface. In addition, to obtain the topological superconductivity in three dimensions, the correct Fermi surface topology is needed.^{5,6,57)}

Next, we consider the pair potentials. We assume that each pair potential is independent of momentum since the present material is not a strongly correlated system.⁵⁷⁾ In this case, the pair potentials are classified into four types of irreducible representation for the D_{3d} point group. The matrix forms of the pairings Δ_1 , Δ_2 , Δ_3 , and Δ_4 are shown in the first column of Table I. Δ_1 and Δ_3 are spin-singlet intra-orbital pairings, whereas Δ_2 and Δ_4 are spin-triplet inter-orbital pairings in the orbital basis. Note that intra-orbital repulsion can be relevant to inter-orbital pairings even though this system is not a strongly correlated system.

We diagonalize the BdG Hamiltonian [eq. (1)]. We obtain four branches of the bulk spectrum E_γ ($\gamma = 1, 2, 3, 4$) for each

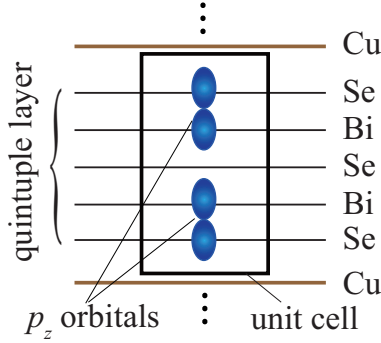


Fig. 1. (Color online) Two p_z orbitals in the quintuple layer of Bi_2Se_3 .

pairing,

$$E_1(\mathbf{k}) = \sqrt{\xi^2(\mathbf{k}) + 2\sqrt{\eta^2(\mathbf{k})c^2(\mathbf{k}) + \zeta^2(\mathbf{k})\Delta^2}}, \quad (15)$$

$$E_2(\mathbf{k}) = \sqrt{\xi^2(\mathbf{k}) - 2\sqrt{\eta^2(\mathbf{k})c^2(\mathbf{k}) + \zeta^2(\mathbf{k})\Delta^2}}, \quad (16)$$

$$E_3(\mathbf{k}) = -\sqrt{\xi^2(\mathbf{k}) + 2\sqrt{\eta^2(\mathbf{k})c^2(\mathbf{k}) + \zeta^2(\mathbf{k})\Delta^2}}, \quad (17)$$

$$E_4(\mathbf{k}) = -\sqrt{\xi^2(\mathbf{k}) - 2\sqrt{\eta^2(\mathbf{k})c^2(\mathbf{k}) + \zeta^2(\mathbf{k})\Delta^2}}, \quad (18)$$

with

$$\eta^2(\mathbf{k}) = m^2(\mathbf{k}) + a_x^2(\mathbf{k}) + a_y^2(\mathbf{k}) + b^2(\mathbf{k}), \quad (19)$$

$$\xi^2(\mathbf{k}) = \eta^2(\mathbf{k}) + c^2(\mathbf{k}) + \Delta^2. \quad (20)$$

The difference in the energy gap structure in each pairing originates from $\zeta^2(\mathbf{k})$,

$$\Delta_1 : \zeta^2(\mathbf{k}) = 0, \quad (21)$$

$$\Delta_2 : \zeta^2(\mathbf{k}) = m^2(\mathbf{k}), \quad (22)$$

$$\Delta_3 : \zeta^2(\mathbf{k}) = m^2(\mathbf{k}) + b^2(\mathbf{k}), \quad (23)$$

$$\Delta_4 : \zeta^2(\mathbf{k}) = m^2(\mathbf{k}) + a_y^2(\mathbf{k}). \quad (24)$$

The energy gap structure of Δ_1 is an isotropic full gap, which is the same as that of conventional BCS superconductors. In other cases, because of the presence of ζ , the energy gap is modified from the BCS gap structure. Δ_2 is an anisotropic full-gap pairing. In the cases of Δ_3 and Δ_4 , the energy gap has point nodes. The point nodes for Δ_3 are on the poles. In the case of Δ_4 , point nodes appear on the k_y -axis. Although, in general, Δ_4 is a linear combination of $\Delta\sigma_y s_x$ and $\Delta\sigma_y s_y$, we can choose $\Delta_4 = \Delta\sigma_y s_x$ without loss of a generality. The energy gap of E_γ is influenced by the spin-orbit interaction v . To elucidate the role of the spin-orbit interaction, we also consider the case of $v = 0$. In this case, E_γ for Δ_1 has a full gap, E_γ for Δ_2 and Δ_4 have line nodes on the equator, and E_γ for Δ_3 is gapless.

pair potential	rep.	spin	orbital	energy gap
$\Delta_1 = \Delta$	A_{1g}	singlet	intra	isotropic full gap (isotropic full gap)
$\Delta_2 = \Delta\sigma_y s_z$	A_{1u}	triplet	inter	anisotropic full gap (line node on equator)
$\Delta_3 = \Delta\sigma_z$	A_{2u}	singlet	intra	point nodes at poles (gapless)
$\Delta_4 = \Delta\sigma_y s_x$	E_u	triplet	inter	point node on equator (line node on equator)

Table I. Irreducible representation, spin state, orbital state and, energy gap structure in each pairing symmetry. In the brackets we denote the gap structure for $v = 0$.

3. Specific Heat

In this section, we calculate the specific heat below T_c for each pairing symmetry. The specific heat is given by

$$\begin{aligned} C_s &= -\frac{2\beta}{N} \sum_{k_y} \left(-\frac{\partial f(E_\gamma(\mathbf{k}))}{\partial E_\gamma(\mathbf{k})} \right) \left(E_\gamma^2(\mathbf{k}) + \frac{\beta}{2} \frac{\partial E_\gamma^2(\mathbf{k})}{\partial \beta} \right) \\ &= -\frac{2\beta}{N} \sum_{k_y} \left(-\frac{\partial f(E_\gamma(\mathbf{k}))}{\partial E_\gamma(\mathbf{k})} \right) \\ &\quad \times \left(E_\gamma^2(\mathbf{k}) + \beta E_\gamma(\mathbf{k}) \frac{\partial \Delta}{\partial \beta} \frac{\partial E_\gamma(\mathbf{k})}{\partial \Delta} \right), \quad (25) \end{aligned}$$

where N is the number of unit cells and β is $1/k_B T$, with the Boltzmann constant k_B and temperature T . We assume that the temperature dependence of the pairing potential is the scaled BCS one, $\Delta(T) = (\alpha/\alpha_{\text{BCS}})\Delta_{\text{BCS}}(T)$. The magnitude of α gives the ratio of $\Delta(T=0)$ to T_c , i.e., $\alpha = \Delta(T=0)/(k_B T_c)$. This model is known as the α -model.⁶⁰ For $\Delta_{\text{BCS}}(T)$, we use the following phenomenological form:⁶¹

$$\Delta_{\text{BCS}}(T) = \alpha_{\text{BCS}} k_B T_c \tanh \left(1.74 \sqrt{\frac{T_c}{T} - 1} \right), \quad (26)$$

with $\alpha_{\text{BCS}} = 1.76$.

Since α is a material-dependent parameter and it often deviates from the BCS value $\alpha_{\text{BCS}} = 1.76$, we use two different values. One is $\alpha = \alpha_{\text{BCS}}$ and the other is $\alpha = \alpha_0$, where $C_s(T)/T$ at $T = 0.53T_c \equiv T_0$ becomes equal to that for the normal state $C_n(T)/T \simeq C_n(T_c)/T_c$ as observed in specific heat measurements.⁴⁵⁾

3.1 Isotropic full gap Δ_1

In Fig. 2, we show the temperature dependence of C_s for $\alpha = \alpha_0 = 1.94$ (blue solid line) and $\alpha = 1.76$ (green dashed line). In the case of Δ_1 , the energy spectrum is given by $E(\mathbf{k}) = \pm \sqrt{\varepsilon_\pm^2(\mathbf{k}) + \Delta^2}$, where $\varepsilon_\pm^2(\mathbf{k})$ is the dispersion of the normal state. Therefore, the energy gap structure becomes an isotropic s -wave one. Thus, the specific heat near $T = 0$ shows exponential behavior. If we choose $\alpha = \alpha_{\text{BCS}}$, T_0 and the magnitude of the specific-heat jump are smaller than those obtained experimentally. To fit the experimental data, we choose

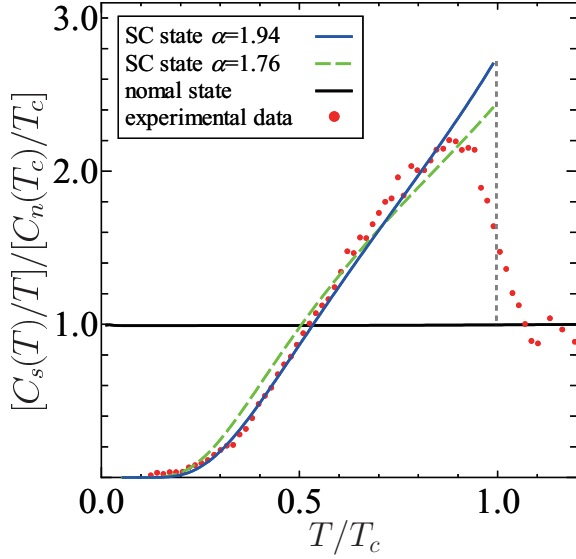


Fig. 2. (Color online) Temperature dependence of specific heat for Δ_1 with $\alpha = 1.94$ (blue solid line) and $\alpha = 1.76$ (green dashed line). The black solid line shows the specific heat for the normal state. Red dotted circles show the experimental data in ref. 45

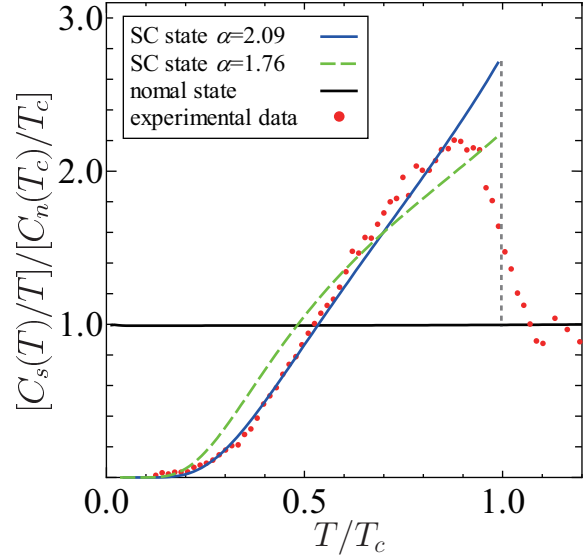


Fig. 3. (Color online) Temperature dependence of specific heat for Δ_2 with $\alpha = 2.09$. The dotted circles show the experimental data in ref. 45.

$\alpha = \alpha_0 = 1.94$. Then, to satisfy the entropy balance relation,

$$\int_0^{T_c} dT \frac{C_s(T) - C_n(T)}{T} = 0, \quad (27)$$

the magnitude of the specific-heat jump at $\alpha = 1.94$ becomes larger than that for $\alpha = \alpha_{\text{BCS}}$.

In the case of $\alpha = \alpha_0$, the magnitude of the specific heat jump and the line shape are similar to those of the experimental ones. Note that the analysis performed in ref. 45 is based on an isotropic s -wave gap and therefore the obtained value of α_0 is almost the same. On the other hand, the value of α can also be estimated from the upper and lower critical field in ref. 45. The estimated value is $\alpha = 2.3 \equiv \alpha_c$. Therefore, the value of α_0 for Δ_1 deviates from that of α_c . However, if we add a small \mathbf{k} -dependent term allowed in the A_{1g} representation to Δ_1 , then the magnitude of the specific heat jump for $\alpha = \alpha_{\text{BCS}}$ can be small, the values of α_0 become large and $\alpha_0 = 2.3$ might be obtained.

3.2 Anisotropic full gap Δ_2

In Fig. 3, we show the temperature dependence of $C_s(T)$ for $\alpha = \alpha_0 = 2.09$ (blue solid line) and $\alpha = 1.76$ (green dashed line). Since the energy gap structure is fully gapped, the exponential behavior appears near $T = 0$ as in the case of Δ_1 . On the other hand, the magnitude of the specific heat jump for $\alpha = \alpha_{\text{BCS}}$ is smaller than that for Δ_1 owing to the anisotropy of the energy gap. Therefore, to reproduce the experimental data, we need a larger value of α_0 than for the case of Δ_1 , $\alpha_0 = 2.09$. This value is closer to $\alpha_c = 2.3$ than that for Δ_1 . The magnitude of the specific heat jump and the line shape

for $\alpha = \alpha_0$ are similar to those of the experimental ones.

3.3 Point nodes at polar Δ_3

In Fig. 4, we show the temperature dependence of $C_s(T)$ for $\alpha = \alpha_0 = 2.74$ (blue solid line) and $\alpha = 1.76$ (green dashed line). In the case of Δ_3 , the energy dispersion has point nodes along the k_z -axis. Thus, $C_s(T)/T$ has T^2 -behavior near $T = 0$. The magnitude of the jump for $\alpha = \alpha_{\text{BCS}}$ is the smallest among the four pair potentials considered in this paper. This small jump originates from the gapless nature of this pair potential. In the case of $\nu = 0$, the energy dispersion for Δ_3 is given by $E(\mathbf{k}) = \pm \sqrt{m^2(\mathbf{k}) + b^2(\mathbf{k})} \pm \sqrt{c(\mathbf{k})^2 + \Delta^2}$. This energy spectrum becomes gapless when $m^2(\mathbf{k}) + b^2(\mathbf{k}) = c(\mathbf{k})^2 + \Delta^2$: The parameters of an STI satisfy the following relations.

$$m_0^2 - \mu^2 - \Delta^2 < 0, \quad (28)$$

$$m_1^2 - c_1^2 > 0, \quad (29)$$

$$m_2^2 - c_2^2 > 0. \quad (30)$$

In this case, the energy spectrum becomes gapless near the Fermi surface in any direction of \mathbf{k} . Thus, $C_s(T)/T$ with $\nu = 0$ is T -independent. In the presence of the spin-orbit interaction, these gapless energy spectra still remain in the direction of the k_z -axis, and point nodes are formed since $a_{x,y}(\mathbf{k}) = 0$ in this direction. In directions other than k_z , the energy gap is generated by the spin-orbit coupling ν , but the gap is smaller than those of the other pairings. Therefore, the T -dependence of $C_s(T)/T$ for $\alpha = \alpha_{\text{BCS}}$ remains relatively small. This is the reason why the specific heat jump is small for Δ_3 compared with that for the other pair potentials. If we use $\alpha = \alpha_0 = 2.74$, we can make the specific heat jump similar to the experimen-

tal one and $[C_s(T_0)/T_0]/[C_n(T_c)/T_c]$ becomes equal to unity. However, the line shape does not reproduce the experimental data. In addition, the value of α_0 is much larger than the experimental value of $\alpha_c = 2.3$.

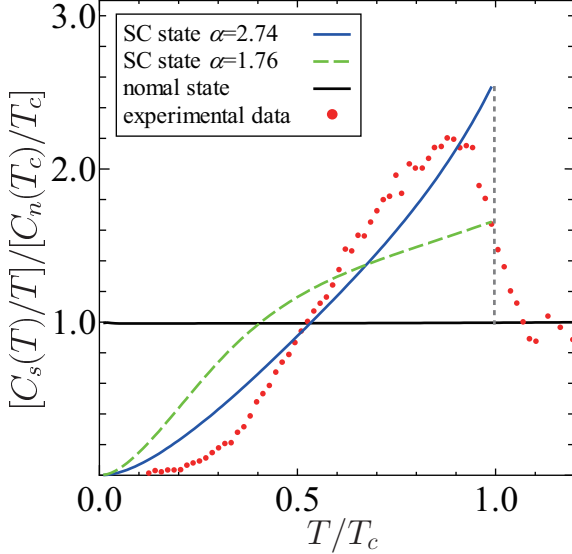


Fig. 4. (Color online) Temperature dependence of specific heat for Δ_3 with $\alpha = 2.74$. The dotted circles show the experimental data in ref. 45.

3.4 Point nodes on equator Δ_4

In Fig. 5, we show the temperature dependence of $C_s(T)$ for $\alpha = \alpha_0 = 2.42$ (blue solid line) and $\alpha = 1.76$ (green dashed line). In the case of Δ_4 , the energy spectrum has point nodes along the k_y -axis. Therefore, $C_s(T)/T$ has T^2 -behavior near $T = 0$ as in the case of Δ_3 . However, in the case of Δ_4 , the energy spectrum does not become gapless even when the spin-orbit interaction is absent. Thus, the coefficient of T^2 is smaller than that in the case of Δ_3 for $\alpha = \alpha_{\text{BCS}}$, and the magnitude of the specific heat jump is larger than that for Δ_3 . As a result, the line shape with $\alpha = \alpha_0 = 2.42$ is considerably closer to the experimental one than in the case of Δ_3 . The obtained value of $\alpha = 2.42$ is the closest to the experimental one, α_c , among the four types of pairing symmetry considered in this paper.

Here, we summarize the results of the specific heat. We have calculated the specific heat for $\alpha = \alpha_{\text{BCS}}$ and α_0 in each pairing symmetry. For $\alpha = \alpha_0$, we obtain line shapes similar to the experimental one in the cases of Δ_1 , Δ_2 , and Δ_4 . The obtained values of α_0 are $\alpha = 1.94, 2.09, 2.74,$ and 2.42 for $\Delta_1, \Delta_2, \Delta_3,$ and Δ_4 , respectively. The values of α for Δ_2 and Δ_4 are closer to the experimental one ($\alpha_c = 2.3$), than for the other pair potentials.

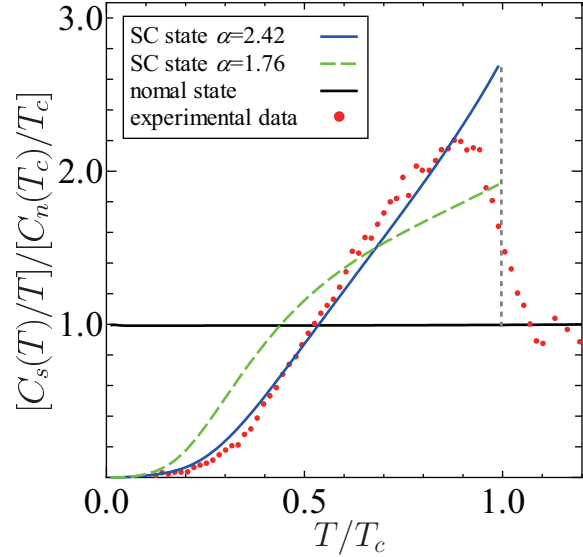


Fig. 5. (Color online) Temperature dependence of specific heat for Δ_4 with $\alpha = 2.42$. The dotted circles show the experimental data in ref. 45.

4. Spin Susceptibility

From the temperature dependence of spin susceptibility, one can determine the spin structure of Cooper pairs. Namely, for a spin-singlet superconductor, the spin susceptibility along any direction decreases with decreasing T for $T < T_c$ and vanishes at $T = 0$. On the other hand, for a spin-triplet superconductor, only the spin susceptibility parallel to the direction of the d -vector decreases with decreasing T and vanishes at $T = 0$, and the spin susceptibility perpendicular to the d -vector is independent of T . However, the temperature dependence of the spin susceptibility of an STI is not simple because spin-singlet and spin-triplet components can mix in the band basis owing to the dependence of the spin-orbit interaction on the pair potential.

Nevertheless, we show here that it is possible to determine the spin structure of an STI, even if the spin-orbit interaction is present. The temperature dependences of spin susceptibility for each possible pairing are different. For Δ_1 , the spin susceptibility along any direction decreases as temperature decreases since Δ_1 is a spin-singlet pair potential in the band basis. On the other hand, that along the z -axis for Δ_3 is independent of temperature, although those along the x - and y -axes decrease with decreasing temperature. Spin susceptibilities with Δ_2 and Δ_4 along the d -vector ($\mathbf{d} \parallel z$ for Δ_2 and $\mathbf{d} \parallel x$ for Δ_4) decrease with decreasing temperature. Those perpendicular to the d -vector are almost independent of temperature.

We now comment on the effects of the spin-orbit interaction on spin susceptibility. There are three effects. The first one is the Van Vleck susceptibility, which originates from inter-band (off-diagonal) matrix elements. The Van Vleck susceptibility can appear in multiband systems with the spin-orbit interaction. This leads to a non zero value of spin susceptibility at

pair potential	effects of SOI
$\Delta_1 = \Delta$	Van Vleck
$\Delta_2 = \Delta\sigma_y s_z$	Van Vleck rotation of d -vector
$\Delta_3 = \Delta\sigma_z$	Van Vleck induced spin-triplet
$\Delta_4 = \Delta\sigma_y s_x$	Van Vleck rotation of d -vector induced spin-singlet

Table II. Summary of effects of spin-orbit interaction on spin susceptibility. The effects of the spin-orbit interaction are the Van Vleck susceptibility, rotation of the d -vector, and the induction of spin-singlet and spin-triplet pair potentials.

$T = 0$ (see Appendix A.1). The second one is the rotation of the d -vector by the unitary transformation from the orbital basis to the band basis, after which the d -vector in the band basis is not parallel to the Zeeman magnetic field, even when the d -vector in the orbital basis is. This also induces a non zero value of spin susceptibility at $T = 0$. Additionally, the spin susceptibility perpendicular to the d -vector in the orbital basis also decreases slightly with decreasing temperature for $T < T_c$. This behavior occurs in the case of Δ_2 and Δ_4 . The third one is the generation of spin-singlet and spin-triplet pair potentials in the band basis from those in the orbital basis, respectively. We summarize these effects for each pairing in Table II. In the following sections, we shall discuss the temperature dependence of the spin susceptibility in each pairing.

4.1 Kubo formula for spin susceptibility

First, we give the Zeeman term in an STI and the Kubo formula for spin susceptibility. The Zeeman term $H_Z(\mathbf{k})$ is given by

$$H_Z(\mathbf{k}) = \sum_{i=x,y,z} \sum_{\mu=0,x,y,z} h_i \mu_B \frac{g_{i\mu}}{2} s_i \sigma_\mu, \quad (31)$$

where μ_B is the Bohr magneton, h_i is the i th component of the Zeeman field, $g_{i\mu}$ is the g -factor of the parent topological insulator, and σ_0 is the 2×2 identity matrix in the orbital space. The spin susceptibility along the i -axis is given by the Kubo formula:

$$\chi_i = -\mu_B^2 \lim_{q \rightarrow 0} \frac{1}{V} \sum_{\mathbf{k}, \alpha, \beta, \mu} \frac{f(E_\alpha(\mathbf{k})) - f(E_\beta(\mathbf{k} + \mathbf{q}))}{E_\alpha(\mathbf{k}) - E_\beta(\mathbf{k} + \mathbf{q}) + i0} \times \langle \alpha | s_i | \beta \rangle \langle \beta | \frac{g_{i\mu}}{2} s_i \sigma_\mu | \alpha \rangle. \quad (32)$$

In the actual calculation, we set $g_{i\mu}$ to be those of Bi_2Se_3 :⁵⁹⁾ $g_{x0} = g_{y0} = -8.92$, $g_{z0} = -21.3$, $g_{xx} = g_{yy} = 0.68$, $g_{zx} = -29.5$. The other g -factors are chosen to be zero. The temperature dependence of Δ is the same as that estimated from the specific heat measurement with $\alpha_c = 2.3$.⁴⁵⁾

4.2 Spin structure in the band basis

In the band basis, spin-singlet and spin-triplet pair potentials can mix with each other because of the spin-orbit interaction. Owing to this, it is rather difficult to understand the temperature dependence of spin susceptibility. In order to clarify the spin structures of pair potentials, it is necessary to introduce the band basis where the normal part of the Hamiltonian is diagonalized. First, we diagonalize the Hamiltonian $H_0(\mathbf{k})$ of the normal state as

$$H_0(\mathbf{k})\mathbf{u}_\gamma(\mathbf{k}) = \epsilon_\gamma(\mathbf{k})\mathbf{u}_\gamma(\mathbf{k}), \quad (33)$$

with band index γ . By using the unitary matrix $U(\mathbf{k})$ given by $U(\mathbf{k}) = (\mathbf{u}_1(\mathbf{k}), \mathbf{u}_2(\mathbf{k}), \dots)$, the pair potential $\hat{\Delta} = \sum_\mu d_\mu s_\mu$ is transformed as

$$\sum_\mu d_\mu s_\mu \rightarrow U^\dagger(\mathbf{k}) \sum_\mu d_\mu s_\mu U(\mathbf{k}) = \sum_\mu \tilde{d}_\mu(\mathbf{k}) s_\mu. \quad (34)$$

$\tilde{d}_0(\mathbf{k})$ and $\tilde{\mathbf{d}}(\mathbf{k})$ denote the spin-singlet component of the pair potential and the d -vector of the spin-triplet component of pair potentials in the band basis, respectively. Note that s_μ is not changed by this unitary transformation in inversion-symmetric systems. The corresponding Hamiltonian is expressed as

$$U^\dagger(\mathbf{k})H(\mathbf{k})U(\mathbf{k}) = \text{diag}(\epsilon_1(\mathbf{k}) - \mu, \epsilon_2(\mathbf{k}) - \mu, \dots) \tau_z + \sum_\mu \tilde{d}_\mu(\mathbf{k}) s_\mu \tau_x. \quad (35)$$

In the following, we give the d -vectors in the band basis for the lowest order of \mathbf{k} . The detailed derivation of $\tilde{d}_\mu(\mathbf{k})$ is shown in Appendix. In the case of Δ_1 , $\tilde{d}_\mu(\mathbf{k})$ is the same as that in the orbital basis: $d_0(\mathbf{k}) = \Delta$, $\mathbf{d}(\mathbf{k}) = \mathbf{0}$. For the other cases, we have

Δ_2 :

$$\tilde{d}_0(\mathbf{k}) = 0, \quad (36)$$

$$\tilde{\mathbf{d}}(\mathbf{k}) = \Delta \left(\frac{vk_x}{m_0}, \frac{vk_y}{m_0}, \frac{v_z k_z}{|m_0|} \tilde{\sigma}_z - \text{sgn}(m_0) \tilde{\sigma}_y \right), \quad (37)$$

Δ_3 :

$$\tilde{d}_0(\mathbf{k}) = \Delta \tilde{\sigma}_x, \quad (38)$$

$$\tilde{\mathbf{d}}(\mathbf{k}) = \Delta \tilde{\sigma}_z \left(-\frac{vk_y}{|m_0|}, \frac{vk_x}{|m_0|}, 0 \right), \quad (39)$$

Δ_4 :

$$\tilde{d}_0(\mathbf{k}) = \Delta \frac{vk_y}{m_0} \frac{v_z k_z}{m_0} \tilde{\sigma}_x, \quad (40)$$

$$\tilde{\mathbf{d}}(\mathbf{k}) = \Delta \left(\frac{v_z k_z}{|m_0|} \tilde{\sigma}_z - \tilde{\sigma}_y, 0, -\frac{vk_x}{m_0} \right), \quad (41)$$

Here, $\tilde{\sigma}_i$ is the Pauli matrix denoting the band index, i.e., $\tilde{\sigma}_z = 1$ for the conduction band and $\tilde{\sigma}_z = -1$ for the valence band. To illustrate $\tilde{\mathbf{d}}(\mathbf{k})$ given by eq. (37) in the conduction (valence) band, we plot the (1, 1)-component [(2, 2)-component] of the $\tilde{\mathbf{d}}$ vector in Fig. 6 (Fig. 7). Those given by

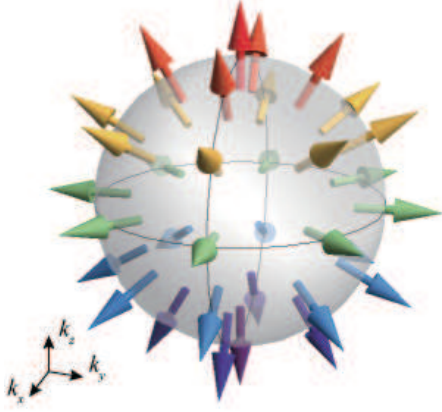


Fig. 6. (Color online) Vector field plot of the conduction-band component of $\vec{d}(\mathbf{k})$ given by eq. 37 for Δ_2 [(1,1)-component].

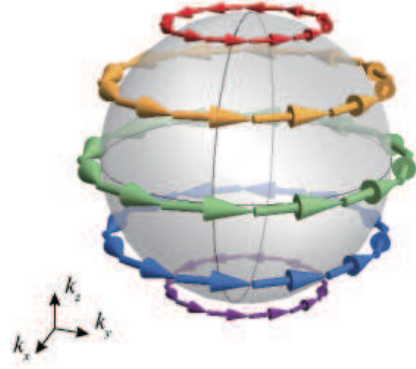


Fig. 8. (Color online) Vector field plot of the conduction-band component of $\vec{d}(\mathbf{k})$ given by eq. 39 for Δ_3 [(1,1)-component].

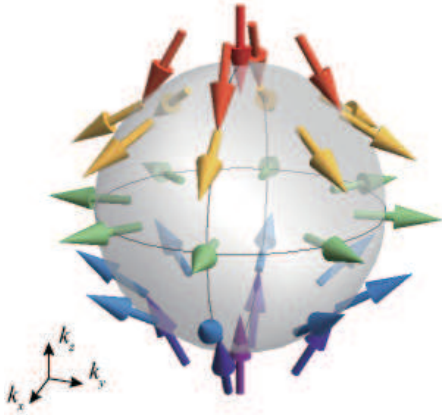


Fig. 7. (Color online) Vector field plot of the valence-band component of $\vec{d}(\mathbf{k})$ given by eq. 37 for Δ_2 [(2,2)-component].

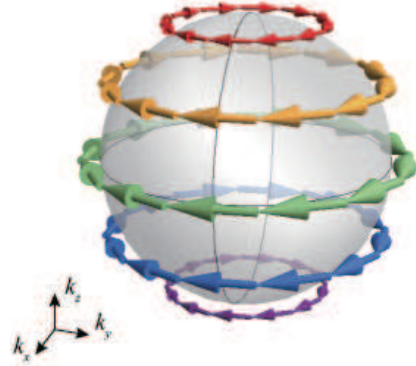


Fig. 9. (Color online) Vector field plot of the valence-band component of $\vec{d}(\mathbf{k})$ given by eq. (39) for Δ_3 [(2,2)-component].

eqs. (39) and (41) are also shown in Figs. 8 and 9 and in Figs. 10 and 11, respectively. $\vec{d}_\mu(\mathbf{k})$ is useful for understanding the temperature dependence of χ_i , as we will see in the following.

4.3 Isotropic full-gap Δ_1 : Van Vleck susceptibility

Figure 12 shows the temperature dependence of χ_i with Δ_1 for $\nu = 3.33 \text{ eV \AA}$ and $\nu = 0$, where ν corresponds to the strength of the spin-orbit interaction. An STI with Δ_1 is a full-gap superconductor, therefore resulting in χ_x, χ_y , and χ_z decreasing exponentially with decreasing T for $T < T_c$ for both $\nu = 0$ and $\nu = 3.33 \text{ eV \AA}$. In the case of $\nu = 0$, all the χ_i vanish at $T = 0$ as shown by the dashed lines in Fig. 12. On the other hand, in the presence of the spin-orbit interaction, all the χ_i remain at a finite value at $T = 0$ (solid line in Fig. 12) owing to the Van Vleck susceptibility,⁶²⁾ which is allowed in a multi band system with the spin-orbit interaction. Actually, χ_z at $T = 0$ is proportional to ν^2 (see Appendix A.1). Note that

the value of χ_z is larger than those of χ_x and χ_y in the normal state because of the anisotropy of the energy band.

4.4 Anisotropic full-gap Δ_2 : Rotation of d -vector

The d -vector in an STI with Δ_2 is parallel to the z -axis in the orbital basis. In the absence of the spin-orbit interaction, the d -vector for Δ_2 in the band basis is also parallel to the z -axis as shown by eq. (37). Consequently, only χ_z decreases with decreasing T and vanishes at $T = 0$, and χ_x and χ_y are independent of T , as shown in Fig. 13. At low temperatures, χ_z is proportional to T since an STI with Δ_2 has a line node on the equator for $\nu = 0$, as discussed in §. 2. In the presence of the spin-orbit interaction, χ_z decreases exponentially with decreasing T for $T < T_c$, as denoted by the solid line in Fig. 13(c). In addition, χ_x and χ_y slightly decrease [solid lines in Figs. 13(a) and 13(b)] with decreasing T since the d -vector is rotated so that the d_x - and d_y -components are induced in the band basis. χ_z at $T = 0$ takes a finite value for the following

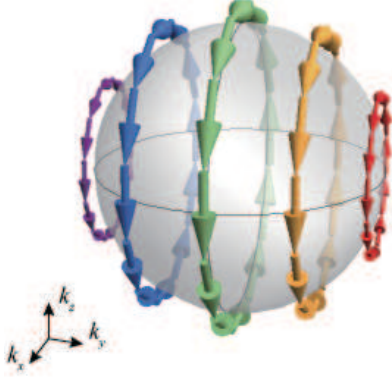


Fig. 10. (Color online) Vector field plot of the conduction-band component of $\tilde{\mathbf{d}}(\mathbf{k})$ given by eq. 41 for Δ_4 [(1,1)-component].

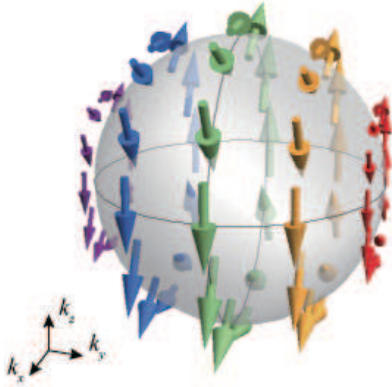


Fig. 11. (Color online) Vector field plot of the valence-band component of $\tilde{\mathbf{d}}(\mathbf{k})$ given by eq. 41 for Δ_4 [(2,2)-component].

two reasons. First, $\tilde{\mathbf{d}}(\mathbf{k})$ is not parallel to the z -axis. Second, the Van Vleck susceptibility arises, as in the case of Δ_1 .

4.5 Point node on poles Δ_3 : Induced spin-triplet pair potential

For $\nu=0$, all the χ_i of an STI with Δ_3 are independent of T , as denoted by the dashed line in Fig. 14, since the energy spectrum is gapless (§3.3). On the other hand, for $\nu = 3.33 \text{ eV\AA}$, χ_x and χ_y decrease with decreasing T to $\chi_i(T=0)/\chi_i(T_c) \sim 0.4$ at $T = 0$ [solid lines in Fig. 14(a)(b)], while χ_z is independent of T [solid line in Fig. 13(c)]. This behavior can be understood from the induced spin-triplet component $\tilde{\mathbf{d}}(\mathbf{k})$ in eq. (39) owing to the spin-orbit interaction. The induced d -vector $\tilde{\mathbf{d}}(\mathbf{k})$ is parallel to the xy -plane, as shown in Figs. 8 and 9; consequently, χ_z becomes independent of T . Moreover, χ_x and χ_y take finite values at $T = 0$ owing to the Van Vleck susceptibility. A similar result has been obtained for a bilayer system.⁶²⁾

pairing potential	specific heat C_s	Andreev bound state	spin susceptibility		
			χ_x	χ_y	χ_z
$\Delta_1 = \Delta$	yes	no	✓	✓	✓
$\Delta_2 = \Delta\sigma_y s_z$	yes	yes	–	–	✓
$\Delta_3 = \Delta\sigma_z$	no	no	✓	✓	–
$\Delta_4 = \Delta\sigma_y s_x$	yes	yes	✓	–	–

Table III. [First column] Possible pairing symmetry of an STI. [Second column] Comparison of line shape between our results and the experimental one.⁴⁵⁾ [Third column] Presence or absence of ZBCP due to ABSs.^{30,34)} [Fourth column] Temperature dependence of χ_x , χ_y , and χ_z . ✓ denotes a decrease in χ_i with decreasing temperature. – denotes that χ_i is almost independent of the temperature.

4.6 Point nodes on equator Δ_4 : Rotation of d -vector and induced spin-singlet pair potential

For $\nu = 0$, because $\tilde{\mathbf{d}}(\mathbf{k}) \parallel \mathbf{x}$ in the band basis, only χ_x decreases with decreasing T for $T < T_c$ and vanishes at $T = 0$ [dashed line in Fig. 15(a)]. At low temperatures, χ_x is proportional to T since the energy spectrum has a line node on the equator (see §. 2). For $\nu = 3.33 \text{ eV\AA}$, χ_x decreases with decreasing T and is proportional to T^2 at low temperatures, except for the residual value at $T = 0$. This residual spin susceptibility originates from the rotated d -vector and the Van Vleck susceptibility due to the spin-orbit interaction. χ_z slightly decreases with decreasing T for $T < T_c$ since $\tilde{\mathbf{d}}_z(\mathbf{k})$ is present. On the other hand, $\tilde{\mathbf{d}}_y(\mathbf{k})$ vanishes up to the first order of \mathbf{k} [eq. (41) and Figs. 10 and 11], and thus χ_y is almost independent of T [solid line in Fig. 15(b)].

5. Discussion and Summary

In this paper, we have calculated the temperature dependence of the specific heat and the spin susceptibility. The temperature dependences of the specific heat are similar among three of the four possible pair potentials. On the other hand, wide variations of the temperature dependence appear in the spin susceptibility depending on the direction of the applied magnetic field. These results are summarized in Table III.

Finally, we compare the obtained results and the experimental ones. From the temperature dependence of the specific heat, Δ_1 , Δ_2 , and Δ_4 are almost consistent with the experimental result. On the other hand, in a recent tunneling spectroscopy investigation of the (111) surface of $\text{Cu}_x\text{Bi}_2\text{Se}_3$, a pronounced ZBCP was observed.³⁴⁾ From the theoretical calculation, the ZBCP due to ABSs is generated on the (111) surface only for the case with Δ_2 and Δ_4 .^{30,34)} On the basis of this background, the promising pair potentials are Δ_2 and Δ_4 . In the light of the obtained spin susceptibility in this paper, we conclude that it is possible to distinguish between Δ_2 and Δ_4 by measuring the temperature dependence of the in-plane and out-of-plane Knight shifts.

6. Acknowledgements

We are grateful to M. Kriener, K. Segawa, Z. Ren, S. Sasaki and Y. Ando for valuable discussions and providing the exper-

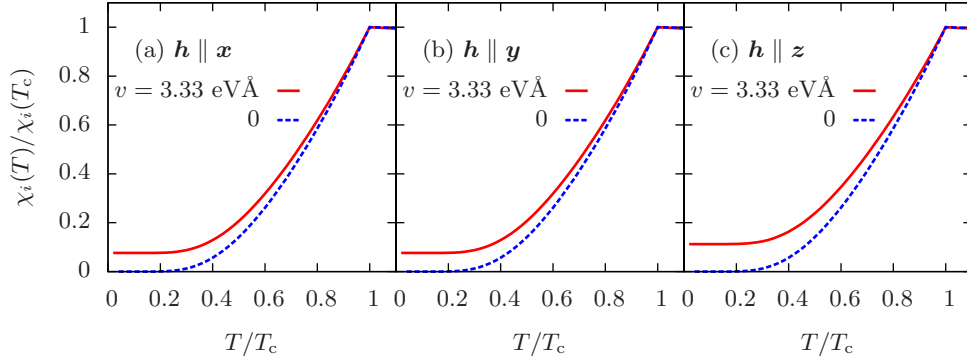


Fig. 12. (Color online) Temperature dependences of spin susceptibilities χ_x (a), χ_y (b), and χ_z (c) of STI with Δ_1 in the presence ($v = 3.33 \text{ eV \AA}$, solid line) and absence ($v = 0$, dashed line) of the spin-orbit interaction. The value of χ_i is normalized by that in the normal state, which is given by $\chi_x(T_c) = \chi_y(T_c) = 0.309\chi_z(T_c)$ for $v = 3.33 \text{ eV \AA}$ and $\chi_x(T_c) = \chi_y(T_c) = 0.210\chi_z(T_c)$ for $v = 0$.

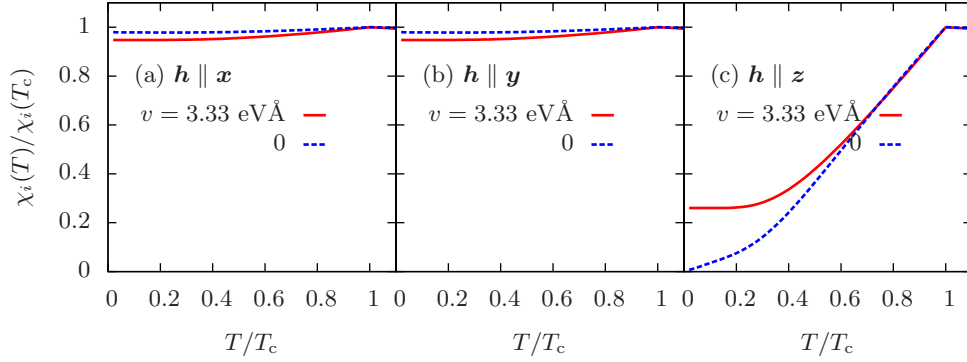


Fig. 13. (Color online) Temperature dependences of spin susceptibilities of STI with Δ_2 .

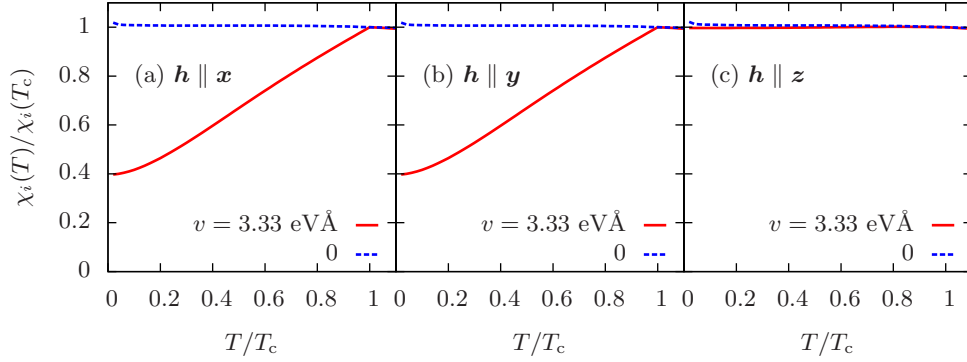


Fig. 14. (Color online) Temperature dependences of spin susceptibilities of STI with Δ_3 .

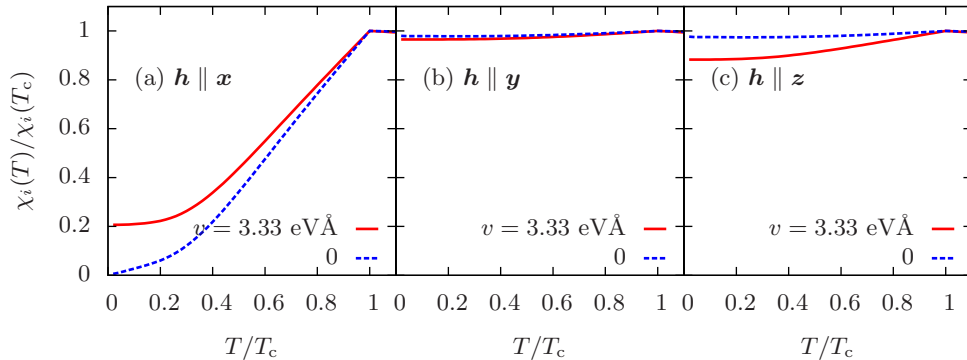


Fig. 15. (Color online) Temperature dependences of spin susceptibilities of STI with Δ_4 .

imental data. We gratefully acknowledge S. Onari for valuable discussions. This work was supported in part by Grants-in-Aid for Scientific Research from MEXT of Japan ‘‘Topological Quantum Phenomena’’ (Grant Nos. 22103005, 20654030 and 22540383).

Appendix: Effects of Spin-Orbit Interaction

A.1 Van Vleck susceptibility for Δ_1

Here, we derive the Van Vleck susceptibility, which gives a finite value of the spin susceptibility at $T = 0$. We focus on an STI with Δ_1 , based on the Hamiltonian in the continuum limit given by

$$H(\mathbf{k}) = [c(\mathbf{k}) + m(\mathbf{k})\sigma_x + v_z k_z \sigma_y + v k_{\parallel} h_s(\mathbf{k})\sigma_z] \tau_z + \Delta \tau_x. \quad (\text{A}\cdot 1)$$

First, we diagonalize the spin part: $h_s(\mathbf{k}) = (\mathbf{k} \times \mathbf{s})_z / k_{\parallel}$, where $k_{\parallel} = |\mathbf{k}_{\parallel}| = (k_x^2 + k_y^2)^{1/2}$. The eigenvalue \tilde{s} of h_s is given by $\tilde{s} = \pm 1$. The corresponding eigenvector is given by

$$|\tilde{s}\rangle = \frac{1}{\sqrt{2}} \begin{pmatrix} 1 \\ \tilde{s} e^{i\varphi_k} \end{pmatrix}, \quad (\text{A}\cdot 2)$$

with $\sin \varphi_k = k_x / k_{\parallel}$ and $\cos \varphi_k = -k_y / k_{\parallel}$.

Next, we diagonalize the normal part: $H_{0\tilde{s}}(\mathbf{k}) = m(\mathbf{k})\sigma_x + v_z k_z \sigma_y + \tilde{s} v k_{\parallel} \sigma_z$. The eigenvalue of $H_{0\tilde{s}}(\mathbf{k})$ is given by $\tilde{\sigma} \eta(\mathbf{k}) + c(\mathbf{k})$ with

$$\eta(\mathbf{k}) = \sqrt{m^2(\mathbf{k}) + v_z^2 k_z^2 + v^2 k_{\parallel}^2}, \quad (\text{A}\cdot 3)$$

where $\tilde{\sigma} = \pm 1$ is the band index. The corresponding eigenvectors $|\tilde{s}\tilde{\sigma}\rangle$ of $H_{0\tilde{s}}(\mathbf{k})$ are given by

$$|\pm, \pm\rangle = \begin{pmatrix} \cos p_k / 2 \\ \pm e^{iq_k} \sin p_k / 2 \end{pmatrix}, \quad (\text{A}\cdot 4)$$

$$|\pm, \mp\rangle = \begin{pmatrix} \sin p_k / 2 \\ \mp e^{iq_k} \cos p_k / 2 \end{pmatrix}, \quad (\text{A}\cdot 5)$$

with

$$\cos p_k = v k_{\parallel} / \eta(\mathbf{k}), \quad (\text{A}\cdot 6)$$

$$\sin p_k = \sqrt{m^2(\mathbf{k}) + v_z^2 k_z^2} / \eta(\mathbf{k}), \quad (\text{A}\cdot 7)$$

$$\cos q_k = m(\mathbf{k}) / \sqrt{m^2(\mathbf{k}) + v_z^2 k_z^2}, \quad (\text{A}\cdot 8)$$

$$\sin q_k = v_z k_z / \sqrt{m^2(\mathbf{k}) + v_z^2 k_z^2}. \quad (\text{A}\cdot 9)$$

In the band basis, the original Hamiltonian is rewritten as

$$H_{\tilde{s}\tilde{\sigma}}(\mathbf{k}) = [\tilde{\sigma} \eta(\mathbf{k}) + c(\mathbf{k})] \tau_z + \Delta \tau_x. \quad (\text{A}\cdot 10)$$

The energy eigenvalue of $H_{\tilde{s}\tilde{\sigma}}(\mathbf{k})$ is given by $\tau E_{\tilde{\sigma}}(\mathbf{k})$ with

$$E_{\tilde{\sigma}}(\mathbf{k}) = \sqrt{[\tilde{\sigma} \eta(\mathbf{k}) + c(\mathbf{k})]^2 + \Delta^2}, \quad (\text{A}\cdot 11)$$

and $\tau = \pm 1$. The corresponding eigenvectors $|\tilde{s}\tilde{\sigma}\tau\rangle$ are given by

$$|\tilde{s}, \tilde{\sigma}, +\rangle = \begin{pmatrix} \cos P_{k\tilde{\sigma}} / 2 \\ \sin P_{k\tilde{\sigma}} / 2 \end{pmatrix}, \quad (\text{A}\cdot 12)$$

$$|\tilde{s}, \tilde{\sigma}, -\rangle = \begin{pmatrix} \sin P_{k\tilde{\sigma}} / 2 \\ -\cos P_{k\tilde{\sigma}} / 2 \end{pmatrix}, \quad (\text{A}\cdot 13)$$

with $\cos P_{k\tilde{\sigma}} = [\tilde{\sigma} \eta(\mathbf{k}) + c(\mathbf{k})] / E_{\tilde{\sigma}}(\mathbf{k})$.

For a full-gap system, the spin susceptibility at $T = 0$ is given by

$$\chi_i = \frac{2\mu_B^2}{N} \sum_{k\tilde{s}\tilde{s}'\tilde{\sigma}\tilde{\sigma}'} \frac{|\langle \tilde{s}|s_i|\tilde{s}'\rangle \langle \tilde{s}, \tilde{\sigma}|\tilde{s}', \tilde{\sigma}'\rangle \langle \tilde{s}, \tilde{\sigma}, +|\tilde{s}', \tilde{\sigma}', -\rangle|^2}{E_{\tilde{\sigma}}(\mathbf{k}) + E_{\tilde{\sigma}'}(\mathbf{k})}. \quad (\text{A}\cdot 14)$$

For simplicity, we assume that all the g -factors are equal to two, and we concentrate on χ_z . The matrix elements in the above expression are estimated as follows.

$$\langle \tilde{s}|s_z|\tilde{s}'\rangle = 1 - \delta_{\tilde{s}\tilde{s}'}, \quad (\text{A}\cdot 15)$$

$$\langle \tilde{s}, \pm | - \tilde{s}, \mp \rangle = \pm \cos p_k, \quad (\text{A}\cdot 16)$$

$$\langle \tilde{s}, \tilde{\sigma}, + | - \tilde{s}, \tilde{\sigma}', - \rangle = \sin \frac{P_{k\tilde{\sigma}'} - P_{k\tilde{\sigma}}}{2}. \quad (\text{A}\cdot 17)$$

From the above equations, only the Van Vleck term, which originates from the off-diagonal terms of $\tilde{s} \neq \tilde{s}'$, $\tilde{\sigma} \neq \tilde{\sigma}'$, and $\tau \neq \tau'$, can be nonzero and is given as

$$\chi_z = \frac{8\mu_B^2}{N} \sum_k \frac{1}{E_+(\mathbf{k}) + E_-(\mathbf{k})} \frac{v^2 k_{\parallel}^2}{\eta^2(\mathbf{k})} \sin^2 \frac{P_{k+} - P_{k-}}{2}. \quad (\text{A}\cdot 18)$$

One can verify that $\chi_z \rightarrow 0$ as $v \rightarrow 0$ from the above expression. The spin susceptibility at $T = 0$ in an STI with Δ_1 stems from the Van Vleck component due to the spin-orbit coupling v .

A.2 Rotation of d -vector for Δ_2

Here, we derive the d -vector for Δ_2 in the band basis. The following relation is useful:

$$\begin{aligned} \langle \tilde{s}, \tilde{\sigma} | \sigma_y | \tilde{s}', \tilde{\sigma}' \rangle &= [\delta_{\tilde{s}\tilde{s}'} (\tilde{\sigma}_z \sin p_k \sin q_k - \tilde{\sigma}_y \cos q_k) \\ &\quad - (\tilde{s}_z)_{\tilde{s}\tilde{s}'} \tilde{\sigma}_x \cos p_k \sin q_k \\ &\quad + (\tilde{s}_x)_{\tilde{s}\tilde{s}'} (\tilde{\sigma}_z \sin q_k - \tilde{\sigma}_y \sin p_k \cos q_k) \\ &\quad + (\tilde{s}_y)_{\tilde{s}\tilde{s}'} \sigma_0 \cos p_k \cos q_k]_{\tilde{\sigma}\tilde{\sigma}'}. \end{aligned} \quad (\text{A}\cdot 19)$$

The above expression is derived using eqs. (A.4) and (A.5). The pair potential Δ_2 is represented in the band basis as

$$\Delta \sigma_y s_z = \Delta (\sin q_k \tilde{\sigma}_z - \cos q_k \sin p_k \tilde{\sigma}_y) \tilde{s}_x + \Delta \cos q_k \frac{v k_{\parallel}}{\eta(\mathbf{k})} \tilde{s}_y, \quad (\text{A}\cdot 20)$$

where \tilde{s}_i is the Pauli matrix in the spin-helicity space. Here, the relation between s and \tilde{s} is as follows:

$$\langle \tilde{s}|s_z|\tilde{s}'\rangle = 1 - \delta_{\tilde{s}\tilde{s}'} = (\tilde{s}_x)_{\tilde{s}\tilde{s}'}, \quad (\text{A}\cdot 21)$$

$$\langle \tilde{s}|s_x|\tilde{s}'\rangle = (\tilde{s}_y)_{\tilde{s}\tilde{s}'} \sin \varphi_k + (\tilde{s}_z)_{\tilde{s}\tilde{s}'} \cos \varphi_k, \quad (\text{A}\cdot 22)$$

$$\langle \tilde{s}|s_y|\tilde{s}'\rangle = (\tilde{s}_z)_{\tilde{s}\tilde{s}'} \sin \varphi_k - (\tilde{s}_y)_{\tilde{s}\tilde{s}'} \cos \varphi_k, \quad (\text{A}\cdot 23)$$

or equivalently,

$$\tilde{s}_x = s_z, \quad (\text{A}\cdot 24)$$

$$\tilde{s}_y = s_x \sin \varphi_k - s_y \cos \varphi_k = \frac{\mathbf{k}_{\parallel} \cdot \mathbf{s}}{k_{\parallel}}, \quad (\text{A}\cdot 25)$$

$$\tilde{s}_z = s_x \cos \varphi_k + s_y \sin \varphi_k = \frac{(\mathbf{k} \times \mathbf{s})_z}{k_{\parallel}}. \quad (\text{A}\cdot 26)$$

Consequently, the d -vector for Δ_2 in the band basis is obtained as

$$\tilde{d}_x(\mathbf{k}) = \Delta \cos q_k \frac{vk_x}{\eta(\mathbf{k})}, \quad (\text{A}\cdot 27)$$

$$\tilde{d}_y(\mathbf{k}) = \Delta \cos q_k \frac{vk_y}{\eta(\mathbf{k})}, \quad (\text{A}\cdot 28)$$

$$\tilde{d}_z(\mathbf{k}) = \Delta(\sin q_k \tilde{\sigma}_z - \cos q_k \sin p_k \tilde{\sigma}_y). \quad (\text{A}\cdot 29)$$

Note that the spin in the above expression is represented in the original spin space (\mathbf{s}) not in the spin-helicity space ($\tilde{\mathbf{s}}$). For an STI with Δ_2 , the spin-orbit interaction has the role of rotating the d -vector in the band basis. In the case of $v = 0$, because $\tilde{\mathbf{d}}(\mathbf{k}) \parallel \mathbf{z}$, only χ_z decreases with decreasing T for $T < T_c$. In the case of $v \neq 0$, $\tilde{d}_x(\mathbf{k})$ and $\tilde{d}_y(\mathbf{k})$ (proportional to v) are present, and χ_x and χ_y also decrease slightly with decreasing T for $T < T_c$.

A.3 Induced spin-triplet pair for Δ_3

In the following, we show that a spin-triplet pair is induced for Δ_3 in the band basis. As in Appendix A.2, we derive $\tilde{\mathbf{d}}(\mathbf{k})$ for $\Delta_3 = \Delta \sigma_z$. Using eqs. (A.4) and (A.5), the matrix elements of σ_z are obtained as

$$\langle \tilde{s}, \tilde{\sigma} | \sigma_z | \tilde{s}, \tilde{\sigma}' \rangle = (\tilde{s} \tilde{\sigma}_z \cos p_k + \tilde{\sigma}_x \sin p_k)_{\tilde{\sigma} \tilde{\sigma}'}. \quad (\text{A}\cdot 30)$$

Therefore, σ_z is expressed in the band basis as

$$\sigma_z = \sin p_k \tilde{\sigma}_x + \frac{v(k_x s_y - k_y s_x)}{\eta(\mathbf{k})} \tilde{\sigma}_z. \quad (\text{A}\cdot 31)$$

This is derived with the help of eq. (A.26). As a result, $\tilde{d}_0(\mathbf{k})$ and $\tilde{\mathbf{d}}(\mathbf{k})$ are given by

$$\tilde{d}_0(\mathbf{k}) = \Delta \sin p_k \tilde{\sigma}_x, \quad (\text{A}\cdot 32)$$

$$\tilde{\mathbf{d}}(\mathbf{k}) = \frac{v\Delta}{\eta(\mathbf{k})} \tilde{\sigma}_z(-k_y, k_x, 0), \quad (\text{A}\cdot 33)$$

which implies that a spin-triplet pair is induced in the band basis. Note that $\tilde{\mathbf{d}}(\mathbf{k}) \perp \mathbf{z}$. This is the reason why almost only χ_z in an STI with Δ_3 decreases with decreasing temperature.

A.4 Induced spin-singlet pair and rotation of d -vector for Δ_4

In this subsection, we derive the d -vector for $\Delta_4 = \Delta \sigma_y s_x$, and show that a spin-singlet pair is induced and that the d -vector is rotated in the band basis. From the matrix elements of σ_y [eq. (A.19)] and s_x [eq. (A.22)], the pair potential Δ_4 in the band basis is represented as follows:

$$\Delta \sigma_y s_x = \Delta \frac{vk_y}{\eta(\mathbf{k})} \sin q_k \tilde{\sigma}_x - \Delta \frac{vk_x}{\eta(\mathbf{k})} \cos q_k \tilde{s}_x$$

$$+ \Delta \frac{k_x}{k_{\parallel}} (\sin q_k \tilde{\sigma}_z - \sin p_k \cos q_k \tilde{\sigma}_y) \tilde{s}_y - \Delta \frac{k_y}{k_{\parallel}} (\sin p_k \sin q_k \tilde{\sigma}_z - \cos q_k \tilde{\sigma}_y) \tilde{s}_z. \quad (\text{A}\cdot 34)$$

Using eqs. (A.24) - (A.26), the d -vector for Δ_4 in the band basis is obtained as

$$\tilde{d}_0(\mathbf{k}) = \Delta \frac{vk_y}{\eta(\mathbf{k})} \sin q_k \tilde{\sigma}_x, \quad (\text{A}\cdot 35)$$

$$\tilde{d}_x(\mathbf{k}) = \Delta \left[\left(\frac{k_y^2}{k_{\parallel}^2} \frac{v_z k_z}{\eta(\mathbf{k})} + \frac{k_x^2}{k_{\parallel}^2} \sin q_k \right) \tilde{\sigma}_z - \left(\frac{k_x^2}{k_{\parallel}^2} \frac{m(\mathbf{k})}{\eta(\mathbf{k})} + \frac{k_y^2}{k_{\parallel}^2} \cos q_k \right) \tilde{\sigma}_y \right], \quad (\text{A}\cdot 36)$$

$$\tilde{d}_y(\mathbf{k}) = \Delta \frac{k_x k_y}{k_{\parallel}^2} \left[\left(\sin q_k - \frac{v_z k_z}{\eta(\mathbf{k})} \right) \tilde{\sigma}_z + \left(\cos q_k - \frac{m(\mathbf{k})}{\eta(\mathbf{k})} \right) \tilde{\sigma}_y \right], \quad (\text{A}\cdot 37)$$

$$\tilde{d}_z(\mathbf{k}) = -\Delta \frac{vk_x}{\eta(\mathbf{k})} \cos q_k. \quad (\text{A}\cdot 38)$$

Therefore, because of the spin-orbit interaction, a spin singlet pair $\tilde{d}_0(\mathbf{k})$ is induced in the band basis, and the d -vector is rotated so that $\tilde{d}_y(\mathbf{k})$ and $\tilde{d}_z(\mathbf{k})$ become nonzero.

-
- 1) M. Z. Hasan and C. L. Kane: Rev. Mod. Phys. **82** (2010) 3045.
 - 2) X.-L. Qi and S.-C. Zhang: Rev. Mod. Phys. **83** (2011) 1057.
 - 3) Y. Tanaka, N. Nagaosa, and M. Sato: J. Phys. Soc. Jpn. **81** (2012) 011013.
 - 4) A. P. Schnyder, S. Ryu, A. Furusaki, and A. W. W. Ludwig: Phys. Rev. B **78** (2008) 195125.
 - 5) M. Sato: Phys. Rev. B **79** (2009) 214526.
 - 6) M. Sato: Phys. Rev. B **81** (2010) 220504(R).
 - 7) F. Wilczek: Nat. Phys. **5** (2009) 614.
 - 8) Y. Maeno, S. Kittaka, T. Nomura, S. Yonezawa, and K. Ishida: J. Phys. Soc. Jpn **81** (2012) 011009.
 - 9) A. P. Mackenzie and Y. Maeno: Rev. Mod. Phys. **75** (2003) 657.
 - 10) A. Furusaki, M. Matsumoto, and M. Sigrist: Phys. Rev. B **64** (2001) 054514.
 - 11) M. Stone and R. Roy: Phys. Rev. B **69** (2004) 184511.
 - 12) S. Kashiwaya, H. Kashiwaya, H. Kambara, T. Furuta, H. Yaguchi, Y. Tanaka, and Y. Maeno: Phys. Rev. Lett. **107** (2011) 077003.
 - 13) Y. Tanaka, T. Yokoyama, A. V. Balatsky, and N. Nagaosa: Phys. Rev. B **79** (2009) 060505.
 - 14) M. Sato and S. Fujimoto: Phys. Rev. B **79** (2009) 094504.
 - 15) M. Sato, Y. Takahashi, and S. Fujimoto: Phys. Rev. Lett. **103** (2009) 020401.
 - 16) M. Sato, Y. Takahashi, and S. Fujimoto: Phys. Rev. B **82** (2010) 134521.
 - 17) M. Sato and S. Fujimoto: Phys. Rev. Lett. **105** (2010) 217001.
 - 18) J. D. Sau, R. M. Lutchyn, S. Tewari, and S. Das Sarma: Phys. Rev. Lett. **104** (2010) 040502.
 - 19) J. Alicea: Phys. Rev. B **81** (2010) 125318.
 - 20) R. M. Lutchyn, J. D. Sau, and S. Das Sarma: Phys. Rev. Lett. **105** (2010) 077001.
 - 21) Y. Oreg, G. Refael, and F. von Oppen: Phys. Rev. Lett. **105** (2010) 177002.
 - 22) R. M. Lutchyn, T. D. Stanescu, and S. Das Sarma: Phys. Rev. Lett. **106** (2011) 127001.

- 23) J. Alicea, Y. Oreg, G. Rafael, F. von Oppen, and M. F. Fisher: *Nat. Phys.* **7** (2011) 412.
- 24) L. Fu and C. L. Kane: *Phys. Rev. Lett.* **100** (2008) 096407.
- 25) L. Fu and C. L. Kane: *Phys. Rev. Lett.* **102** (2009) 216403.
- 26) A. R. Akhmerov, J. Nilsson, and C. W. J. Beenakker: *Phys. Rev. Lett.* **102** (2009) 216404.
- 27) K. T. Law, P. A. Lee, and T. K. Ng: *Phys. Rev. Lett.* **103** (2009) 237001.
- 28) Y. Tanaka, T. Yokoyama, and N. Nagaosa: *Phys. Rev. Lett.* **103** (2009) 107002.
- 29) J. Linder, Y. Tanaka, T. Yokoyama, A. Sudbø, and N. Nagaosa: *Phys. Rev. Lett.* **104** (2010) 067001.
- 30) A. Yamakage, K. Yada, M. Sato, and Y. Tanaka: *Phys. Rev. B* **85** (2012) 180509.
- 31) A. Yamakage, Y. Tanaka, and N. Nagaosa: *Phys. Rev. Lett.* **108** (2012) 087003.
- 32) C. W. J. Beenakker: arXiv:1112.1950 .
- 33) Y. S. Hor, A. J. Williams, J. G. Checkelsky, P. Roushan, J. Seo, Q. Xu, H. W. Zandbergen, A. Yazdani, N. P. Ong, and R. J. Cava: *Phys. Rev. Lett.* **104** (2010) 057001.
- 34) S. Sasaki, M. Kriener, K. Segawa, K. Yada, Y. Tanaka, M. Sato, and Y. Ando: *Phys. Rev. Lett.* **107** (2011) 217001.
- 35) C. R. Hu: *Phys. Rev. Lett.* **72** (1994) 1526.
- 36) Y. Tanaka and S. Kashiwaya: *Phys. Rev. Lett.* **74** (1995) 3451.
- 37) S. Kashiwaya and Y. Tanaka: *Rep. Prog. Phys.* **63** (2000) 1641.
- 38) L. Hao and T. K. Lee: *Phys. Rev. B* **83** (2011) 134516.
- 39) T. H. Hsieh and L. Fu: *Phys. Rev. Lett.* **108** (2012) 107005.
- 40) G. Koren, T. Kirzhner, E. Lahoud, K. B. Chashka, and A. Kanigel: *Phys. Rev. B* **84** (2011) 224521.
- 41) G. Koren and T. Kirzhner: *Phys. Rev. B* **86** (2012) 144508.
- 42) N. Levy, T. Zhang, J. Ha, F. Sharifi, A. A. Talin, Y. Kuk, and J. A. Stroscio: arXiv:1211.0267 .
- 43) L. A. Wray, S.-Y. Xu, Y. Xia, D. Qian, A. V. Fedorov, H. Lin, A. Bansil, L. Fu, Y. S. Hor, R. J. Cava, and M. Z. Hasan: *Nat. Phys.* **6** (2010) 855.
- 44) L. A. Wray, S. Xu, Y. Xia, D. Qian, A. V. Fedorov, H. Lin, A. Bansil, L. Fu, Y. S. Hor, R. J. Cava, and M. Z. Hasan: *Phys. Rev. B* **83** (2011) 224516.
- 45) M. Kriener, K. Segawa, Z. Ren, S. Sasaki, and Y. Ando: *Phys. Rev. Lett.* **106** (2011) 127004.
- 46) M. Kriener, K. Segawa, Z. Ren, S. Sasaki, S. Wada, S. Kuwabata, and Y. Ando: *Phys. Rev. B* **84** (2011) 054513.
- 47) P. Das, Y. Suzuki, M. Tachiki, and K. Kadowaki: *Phys. Rev. B* **83** (2011) 220513.
- 48) M. Kriener, K. Segawa, S. Sasaki, and Y. Ando: *Phys. Rev. B* **86** (2012) 180505.
- 49) Y. Nagai, H. Nakamura, and M. Machida: *Phys. Rev. B* **86** (2012) 094507.
- 50) D. J. Scalapino: *Phys.Rep.* **250** (1995) 329.
- 51) M. Sigrist and T. M. Rice: *Rev. Mod. Phys.* **67** (1995) 503.
- 52) C. C. Tsuei and J. R. Kirtley: *Rev. Mod. Phys.* **72** (2000) 969.
- 53) T. Nomura and K. Yamada: *J. Phys. Soc. Jpn.* **71** (2002) 404.
- 54) M. E. Zhitomirsky and T. M. Rice: *Phys. Rev. Lett.* **87** (2001) 057001.
- 55) H. Tou, Y. Kitaoka, K. Ishida, K. Asayama, N. Kimura, Y. Onuki, E. Yamamoto, Y. Haga, and K. Maezawa: *Phys. Rev. Lett.* **80** (1998) 3129.
- 56) K. Machida and M. Ichioka: *Phys. Rev. B* **77** (2008) 184515.
- 57) L. Fu and E. Berg: *Phys. Rev. Lett.* **105** (2010) 097001.
- 58) H. Zhang, C.-X. Liu, X.-L. Qi, X. Dai, Z. Fang, and S.-C. Zhang: *Nature Phys.* **5** (2009) 438.
- 59) C.-X. Liu, X.-L. Qi, H. Zhang, X. Dai, Z. Fang, and S.-C. Zhang: *Phys. Rev. B* **82** (2010) 045122.
- 60) H. Padamsee, J. E. Neighbor, and C. A. Shiffman: *J. Low Temp. Phys.* **12** (1973) 387.
- 61) B. Mühlischlegel: *Z. Phys.* **155** (1959) 313.
- 62) D. Maruyama, M. Sigrist, and Y. Yanase: *J. Phys. Soc. Jpn.* **81** (2012) 034702.